Disclosing large-scale directed functional connections in MEG with the multivariate phase slope index

Alessio Basti [a], Vittorio Pizzella [a,b], Federico Chella [a,b], Gian Luca Romani [b], Guido Nolte [c], Laura Marzetti [a,b,*]

[a] Department of Neuroscience, Imaging and Clinical Sciences, "G. d'Annunzio" University of Chieti-Pescara, 66100, Chieti, Italy
[b] Institute for Advanced Biomedical Technologies, "G. d'Annunzio" University of Chieti-Pescara, 66100, Chieti, Italy
[c] Department of Neurophysiology and Pathophysiology, University Medical Center Hamburg-Eppendorf, D-20246 Hamburg, Germany

ARTICLE INFO

ABSTRACT

The phase slope index (PSI) is a method to disclose the direction of frequency-specific neural interactions from magnetoencephalographic (MEG) time series. A fundamental property of PSI is that of vanishing for linear mixing of independent neural sources. This property allows PSI to cope with the artificial instantaneous connectivity among MEG sensors or brain sources induced by the field spread. Nevertheless, PSI is limited by being a bivariate estimator of directionality as opposite to the multidimensional nature of brain activity as revealed by MEG. The purpose of this work is to provide a multivariate generalization of PSI. We termed this measure as the multivariate phase slope index (MPSI). In order to test the ability of MPSI in estimating the directionality, and to compare the MPSI results to those obtained by bivariate PSI approaches based on maximizing imaginary part of coherency and on canonical correlation analysis, we used extensive simulations. We proved that MPSI achieves the highest performance and that in a large number of simulated cases, the bivariate methods, as opposed to MPSI, do not detect a statistically significant directionality. Finally, we applied MPSI to assess seed-based directed functional connectivity in the alpha band from resting state MEG data of 61 subjects from the Human Connectome Project. The obtained results highlight a directed functional coupling in the alpha band between the primary visual cortex and several key regions of well-known resting state networks, e.g. dorsal attention network and fronto-parietal network.

Introduction

Systems neuroscience studies in the last decade have made clear that normal brain function requires the concurrent and synergic cooperation of several segregated areas (Deco et al., 2015; Sporns, 2013). Indeed, the putative coordinating mechanism supporting brain inter-areal functional cooperation is the phase locking of brain oscillatory activity, i.e., of brain rhythms (Engel et al., 2013; Hillebrand et al., 2016; Varela et al., 2001). Understanding the resulting large-scale network organization of the brain has thus become crucial to disclose brain functioning. To this end, a non invasive measurement of electrophysiological activity with millisecond time resolution, such as magnetoencephalography (MEG) or electroencephalography (EEG), is needed to characterize synchronization among brain sources at a time scale relevant to behaviour, i.e. occurring with subsecond timing and at frequencies in the range 1–100 Hz.

The reliable estimation of functional connections between brain areas from MEG/EEG data requires methods able to cope with the negative effects of field spread,[1] i.e. the artificial instantaneous coupling between measurement sensors or brain sources. In fact, the resulting artificial connectivity cannot be eliminated even by solving an electromagnetic inverse problem to infer source activities from sensor data.

Several computational approaches have been designed and successfully used to capture the different aspects of inter-areal synchronization bearing in mind their ability to face field spread effects (Brookes et al., 2012; Colclough et al., 2015; Ewald et al., 2012; Hipp et al., 2012; Marzetti et al., 2008; Nolte et al., 2004, 2009; Soto et al., 2016; Vinck et al., 2011). In this framework, a key aspect of inter-areal synchronization is the directionality of the coupling. Namely, it is important not only to know that brain area A is coupled to brain area B but also if brain area A leads brain area B or vice versa. This knowledge is crucial to

---

unravel the complex mechanisms that guide dynamic network instantiation during cognitive processing in humans, e.g. to disambiguate feedback versus feedforward control.

Among the possible different approaches used to estimate directional coupling between brain areas, a promising approach relies on the temporal delays that occur because of the finite speed of information (Bastos et al., 2015; Fries, 2015). Indeed, to estimate the directionality of frequency-specific coupling in a way robust to the field spread effects, the phase slope index (PSI) has been developed (Nolte et al., 2008). PSI is a bivariate estimator that detects the coupling direction by relying on the sign of the discrete derivative with respect to frequency of the phase difference between two time series, e.g. source activities, this derivative being proportional to the time delay between them (Nolte et al., 2008; Basti et al., 2017). The bivariate nature of the PSI imposes that this measure is able to detect the directionality from a pair of scalar, i.e. one-dimensional, time series. Thus, when used to assess directionality between brain sources estimated from MEG/EEG data, the vector source activity must be reduced to a scalar one, prior to applying PSI. This is usually accomplished by fixing, for each brain source, a preferential direction for its activity, e.g. geometrical direction normal to the cortical surface, or functional direction such as that of maximum source power. Nevertheless, this dimensionality reduction might be suboptimal when connectivity is at target, as already shown for non-directed bivariate measures when source direction is fixed according to a maximum power criterion (Marzetti et al., 2013). Moreover, choosing a geometrical approach in fixing the direction can also be misleading if, e.g., coregistration errors or distortions in the reference anatomical image are present.

Purpose and structure of the work

In this paper, we will provide the definition of a multivariate measure[2] based on the concept of PSI, namely the multivariate phase slope index (MPSI), which overcomes the need for dimensionality reduction prior to PSI estimation in a way robust to the negative field spread effects. Specifically, the purpose of this work is to: i) provide the definition of MPSI; ii) demonstrate MPSI performance in detecting the directionality of coupling in extensive and biologically realistic simulations based on synthetic multivariate time series; iii) derive frequency-specific directed networks in a real data application, i.e., resting state data from 61 subjects of the Human Connectome Project (HCP) MEG database.

The paper is organized as follows. In the "Methods" section, we will briefly review the mathematical formulation of the bivariate PSI, as originally introduced in Nolte et al. (2008), and we will provide a new generalized formulation for the multivariate case by introducing a blockwise approach. In the "Experiments" section, we will describe the experiments performed in this work: the simulation studies to evaluate the reliability of MPSI in detecting the right directionality in multivariate interactions in synthetic data, and the real data study to assess seed-based directed functional connectivity in resting state MEG data from the HCP database. Results for MPSI in both synthetic and real data will be compared to the results of two measures based on the bivariate PSI in which scalar information are derived either by canonical correlation analysis (Hotelling, 1936) or by maximizing the imaginary part of coherency (Ewald et al., 2012). The results for the experiments and for the different approaches are described and discussed in the "Results" and the "Discussion" sections.

Methods

Bivariate phase slope index

The PSI (Nolte et al., 2008) is a measure of directionality of coupling between brain areas based on the spectral properties of electrophysiological data. Specifically, it estimates which is the leading source in a pair by relying on the sign of the discrete frequency derivative of the phase difference between two signals. The PSI between two given scalar signals z_1 and z_2 over the set of frequencies of interest F, is defined as

$$\text{PSI} := \mathfrak{I}\left(\sum_{f \in F} \frac{s_{z_1, z_2}(f + \mathrm{d}f)}{\sqrt{s_{z_1, z_1}(f + \mathrm{d}f) s_{z_2, z_2}(f + \mathrm{d}f)}} \frac{s^*_{z_1, z_2}(f)}{\sqrt{s_{z_1, z_1}(f) s_{z_2, z_2}(f)}} \right) \tag{1}$$

where $\mathfrak{I}$ is the imaginary part, the symbol $*$ denotes the complex conjugate, $\mathrm{d}f$ is an incremental step in the frequency domain, and, e.g., s_{z_1, z_2} is the cross-spectrum between z_1 and z_2. That is,

$$s_{z_1, z_2}(f) := \left\langle \widehat{z}_1(f) \widehat{z}^*_2(f) \right\rangle, \tag{2}$$

where $< \cdot >$ denotes the expectation value.

A fundamental property of PSI is that it vanishes for linear mixtures of independent sources (see Appendix A). This property makes PSI robust to the artificial connectivity induced by the field spread when PSI is used to disclose the direction of bivariate interactions from sensor signals or from source time series.

Definition of the multivariate phase slope index

In this subsection, we will introduce a multivariate generalization of the bivariate PSI. To this end, we will firstly define the vector time series of interest and, then, we will: 1) transform them by using a spatial whitening based on the real part of their cross-spectra; 2) apply an averaging process based on the calculations of PSI between all the possible combination of the transformed signals. This procedure will allow us to obtain a multivariate estimator of directionality that will be invariant under invertible linear static transformations of the vector time series, such as rotations of the physical reference frame.

Let us consider two data spaces A and B of dimensions N_A and N_B[3] with the associated vector time series $Z_A = (z_1, \ldots, z_{N_A})^t$ and $Z_B = (z_{N_A+1}, \ldots, z_{N_A+N_B})^t$, where t denotes the transposition. For instance, the data spaces could represent the three-dimensional dipole moments at two brain locations and thus they would have dimensions $N_A = N_B = 3$, or they could indicate two different groups of electrophysiological sensors and thus N_A and N_B would be equal to the number of sensors of each data space.

Now, let us suppose to be interested in investigating the directionality of a frequency-specific interaction between A and B from the time series Z_A and Z_B.

These real valued time courses can be written in the frequency domain and, at a given frequency $f \in F$ with F being the set of frequencies of interest, they are described by the complex vectors $\widehat{Z}_A(f) = (\widehat{z}_1(f), \ldots, \widehat{z}_{N_A}(f))^t$, $\widehat{Z}_B(f) = (\widehat{z}_{N_A+1}(f), \ldots, \widehat{z}_{N_A+N_B}(f))^t$ representing their Fourier transforms. For the sake of simplicity, it is convenient to put them together by using the following compact notation

$$\widehat{Z}(f) = \left[\widehat{Z}_A(f)^t \quad \widehat{Z}_B(f)^t \right]^t. \tag{3}$$

The complex cross-spectral matrix of Z, namely $\mathbf{S}(f)$, shows the following block form:

$$\mathbf{S}(f) = \langle \widehat{Z}(f)\widehat{Z}(f)^H \rangle = \begin{pmatrix} \langle \widehat{Z}_A(f)\widehat{Z}_A(f)^H \rangle & \langle \widehat{Z}_A(f)\widehat{Z}_B(f)^H \rangle \\ \langle \widehat{Z}_B(f)\widehat{Z}_A(f)^H \rangle & \langle \widehat{Z}_B(f)\widehat{Z}_B(f)^H \rangle \end{pmatrix}$$

$$= \begin{pmatrix} S_{AA}^R(f) + iS_{AA}^I(f) & S_{AB}^R(f) + iS_{AB}^I(f) \\ S_{BA}^R(f) + iS_{BA}^I(f) & S_{BB}^R(f) + iS_{BB}^I(f) \end{pmatrix}, \tag{4}$$

with H denoting the Hermitian transpose of a matrix, the apexes R and I the real and the imaginary part, respectively. Each of the four sub-matrices represents the complex cross-spectrum between the corresponding vector time series.

Now, let us transform the vector Z by using the matrix defined as

$$T(f) = \begin{pmatrix} \left(\dfrac{S_{AA}^R(f) + S_{AA}^R(f+\mathrm{d}f)}{2}\right)^{-\frac{1}{2}} & 0_{AB} \\ 0_{BA} & \left(\dfrac{S_{BB}^R(f) + S_{BB}^R(f+\mathrm{d}f)}{2}\right)^{-\frac{1}{2}} \end{pmatrix}, \tag{5}$$

where $\mathrm{d}f$ is an incremental step in the frequency domain and 0_{AB}, 0_{BA} denote the zero matrices of $\mathbf{R}^{N_A \times N_B}$ and $\mathbf{R}^{N_B \times N_A}$. The matrix $T(f)$ is a spatial whitening transformation which completely removes the average contribution of the real parts of cross-spectra at the frequencies f and $f + \mathrm{d}f$ within the data spaces A and B and which normalizes the average power spectra. Indeed, if we define the transformed frequency dependent data as $\widehat{U}(f) = (\widehat{u}_1(f), ..., \widehat{u}_{N_A+N_B}(f))^t = T(f)\widehat{Z}(f)$, for the frequency f, and as $\widehat{V}(f+\mathrm{d}f) = (\widehat{v}_1(f+\mathrm{d}f), ..., \widehat{v}_{N_A+N_B}(f+\mathrm{d}f))^t = T(f)\widehat{Z}(f+\mathrm{d}f)$, for $f + \mathrm{d}f$, we have that

$$\Re\left(\langle \widehat{U}(f)\widehat{U}(f)^H \rangle + < \widehat{V}(f+\mathrm{d}f)\widehat{V}(f+\mathrm{d}f)^H >\right)/2 = \Re\left(T(f)\left(<\widehat{Z}(f)\widehat{Z}(f)^H > + \right.\right.$$
$$\left.\left. <\widehat{Z}(f+\mathrm{d}f)\widehat{Z}(f+\mathrm{d}f)^H >\right)T(f)^t\right)/2$$
$$= \begin{pmatrix} Id_{AA} & \dfrac{C_{AB}^R(f) + D_{AB}^R(f+\mathrm{d}f)}{2} \\ \dfrac{(C_{BA}^R(f) + D_{BA}^R(f+\mathrm{d}f))}{2} & Id_{BB} \end{pmatrix} \tag{6}$$

where $\Re$ is the real part, Id_{AA} is the identity matrix of dimension N_A and, e.g., the matrices C_{AB}^R, D_{AB}^R denote, respectively, the real part of the cross-spectrum between U_A and U_B and between V_A and V_B. In particular, by applying $T(f)$ we obtain that the average of the power spectra at f and $f + \mathrm{d}f$ of all the transformed scalar time series are exactly equal to 1. Indeed, by indicating with $e_1 = (1, ..., 0)^t$ a standard vector of $\mathbf{R}^{N_A}$, we have that

$$\left(\langle \widehat{u}_1(f)\widehat{u}_1^*(f) \rangle + < \widehat{v}_1(f+\mathrm{d}f)\widehat{v}_1^*(f+\mathrm{d}f) >\right)/2 = e_1^t\left(\left(<\widehat{U}_A(f)\widehat{U}_A(f)^H > + \right.\right.$$
$$\left.\left. < \widehat{V}_A(f+\mathrm{d}f)\widehat{V}_A(f+\mathrm{d}f)^H >\right)/2\right)e_1$$
$$= e_1^t\left(Id_{AA} + i\left(C_{AA}^I(f) + D_{AA}^I(f+\mathrm{d}f)\right)/2\right)e_1 = ||e_1||^2 = 1. \tag{7}$$

Even though the spatial whitening normalizes the average power contribution at f and $f + \mathrm{d}f$, it does not guarantee that the power gets exactly flat at both the two frequencies. In fact, by using a single spatial transformation it is not possible to guarantee flatness for both frequencies, and the use of multiple spatial transformations would not lead to the invariance of the resulting metric under invertible linear static transformations of the data. Thus, the use of the matrix $T(f)$ is a way to normalize the data at the two frequencies by relying on a single transformation and, at the same time, to have rotational invariance.

To the final aim of introducing the multivariate version of PSI, let us now apply an averaging process based on the sum, over all possible combinations, of the unnormalized bivariate PSIs between the transformed scalar time courses. Indeed, given that the spatial whitening has already allowed us to remove possible biases induced by source powers, we do not need to use the PSI normalization factor, which would be equal to the square root of the product of power-spectra (see (1)) and which

would not guarantee invariance under rotations of the reference frame. Specifically,

$$\sum_{f \in F}\sum_{i=1}^{N_A}\sum_{j=1}^{N_B}\mathfrak{I}\left(s_{e_i^t V_A, e_j^t V_B}(f+\mathrm{d}f)s^*_{e_i^t U_A, e_j^t U_B}(f)\right)$$

$$= \sum_{f \in F}\sum_{i=1}^{N_A}\sum_{j=1}^{N_B}\mathfrak{I}\left(e_i^t\langle \widehat{V}_A(f+\mathrm{d}f)\widehat{V}_B(f+\mathrm{d}f)^H \rangle e_j\left(e_i^t\langle \widehat{U}_A(f)\widehat{U}_B(f)^H \rangle e_j\right)^*\right)$$

$$= \sum_{f \in F}\sum_{i=1}^{N_A}\sum_{j=1}^{N_B}\mathfrak{I}\left(e_i^t\langle \widehat{V}_A(f+\mathrm{d}f)\widehat{V}_B(f+\mathrm{d}f)^H \rangle e_j e_j^t\langle \widehat{U}_B(f)\widehat{U}_A(f)^H \rangle e_i\right)$$

$$= \sum_{f \in F}\sum_{i=1}^{N_A}e_i^t\left(\sum_{j=1}^{N_B}D_{AB}^I(f+\mathrm{d}f)e_j e_j^t C_{BA}^R(f) + D_{AB}^R(f+\mathrm{d}f)e_j e_j^t C_{BA}^I(f)\right)e_i$$

$$= \sum_{f \in F}\sum_{i=1}^{N_A}e_i^t\left(D_{AB}^I(f+\mathrm{d}f)\left(\sum_{j=1}^{N_B}e_j \otimes e_j^t\right)C_{BA}^R(f)\right.$$
$$\left. + D_{AB}^R(f+\mathrm{d}f)\left(\sum_{j=1}^{N_B}e_j \otimes e_j^t\right)C_{BA}^I(f)\right)$$

$$= \sum_{f \in F}\sum_{i=1}^{N_A}e_i^t\left(D_{AB}^I(f+\mathrm{d}f)C_{BA}^R(f) + D_{AB}^R(f+\mathrm{d}f)C_{BA}^I(f)\right)e_i$$

$$= \sum_{f \in F}\mathrm{tr}\left(D_{AB}^I(f+\mathrm{d}f)C_{BA}^R(f) + D_{AB}^R(f+\mathrm{d}f)C_{BA}^I(f)\right) \tag{8}$$

where we used that $\sum_{j=1}^{N_B}e_j \otimes e_j^t = Id_B$, with the symbol $\otimes$ denoting the tensor product. By using the definitions of the spectral matrices of U, V and by using the properties of the trace, it is thus possible to write the quantity defined in (8) as a function of only the cross-spectral matrices of Z_A and Z_B defined in (4). In fact, $\forall f \in F$

$$\mathrm{tr}\left(D_{AB}^I(f+\mathrm{d}f)C_{BA}^R(f) + D_{AB}^R(f+\mathrm{d}f)C_{BA}^I(f)\right)$$
$$= \mathrm{tr}\left(\left((S_{AA}^R(f) + S_{AA}^R(f+\mathrm{d}f))/2\right)^{-1}S_{AB}^I(f+\mathrm{d}f)\right.$$
$$\cdot\left((S_{BB}^R(f) + S_{BB}^R(f+\mathrm{d}f))/2\right)^{-1}\cdot S_{BA}^R(f) + \left((S_{AA}^R(f) + S_{AA}^R(f+\mathrm{d}f))/2\right)^{-1}$$
$$\left.\cdot S_{AB}^R(f+\mathrm{d}f)\cdot\left((S_{BB}^R(f) + S_{BB}^R(f+\mathrm{d}f))/2\right)^{-1}\cdot S_{BA}^I(f)\right). \tag{9}$$

Finally, by using that for two given matrices M_1 and M_2 it holds that $(M_1/2)^{-1}\cdot(M_2/2)^{-1} = 4\cdot(M_1^{-1}\cdot M_2^{-1})$, we can introduce the multivariate phase slope index (MPSI) between A and B as

$$\mathrm{MPSI}_{AB} := 4\cdot\mathrm{tr}\left(\sum_{f \in F}\left(S_{AA}^R(f) + S_{AA}^R(f+\mathrm{d}f)\right)^{-1}\cdot S_{AB}^I(f+\mathrm{d}f)\right.$$
$$\cdot\left(S_{BB}^R(f) + S_{BB}^R(f+\mathrm{d}f)\right)^{-1}\cdot S_{BA}^R(f) + \left(S_{AA}^R(f) + S_{AA}^R(f+\mathrm{d}f)\right)^{-1}$$
$$\left.\cdot S_{AB}^R(f+\mathrm{d}f)\cdot\left(S_{BB}^R(f) + S_{BB}^R(f+\mathrm{d}f)\right)^{-1}\cdot S_{BA}^I(f)\right) \tag{10}$$

The equation (10) thus represents a multivariate phase slope based approach to assess the directionality of the frequency-specific multivariate interaction between A and B.

MPSI exhibits three properties which hold by construction:

1) it can directly assess the directionality of frequency-specific interactions without relying on dimensionality reduction approaches, as opposed to bivariate PSI (Fig. 1);
2) it vanishes for linear mixture of independent sources, analogously to bivariate PSI. The proof of this property can be found in Appendix A;
3) it is invariant under invertible linear static transformations of the data such as rotations of the data spaces A and B. Thus, MPSI is independent of the choice of the three-dimensional reference frame in which e.g. the MEG source space is defined. The proof of this property can be found in Appendix B, while two computational examples are provided in Fig. 2.
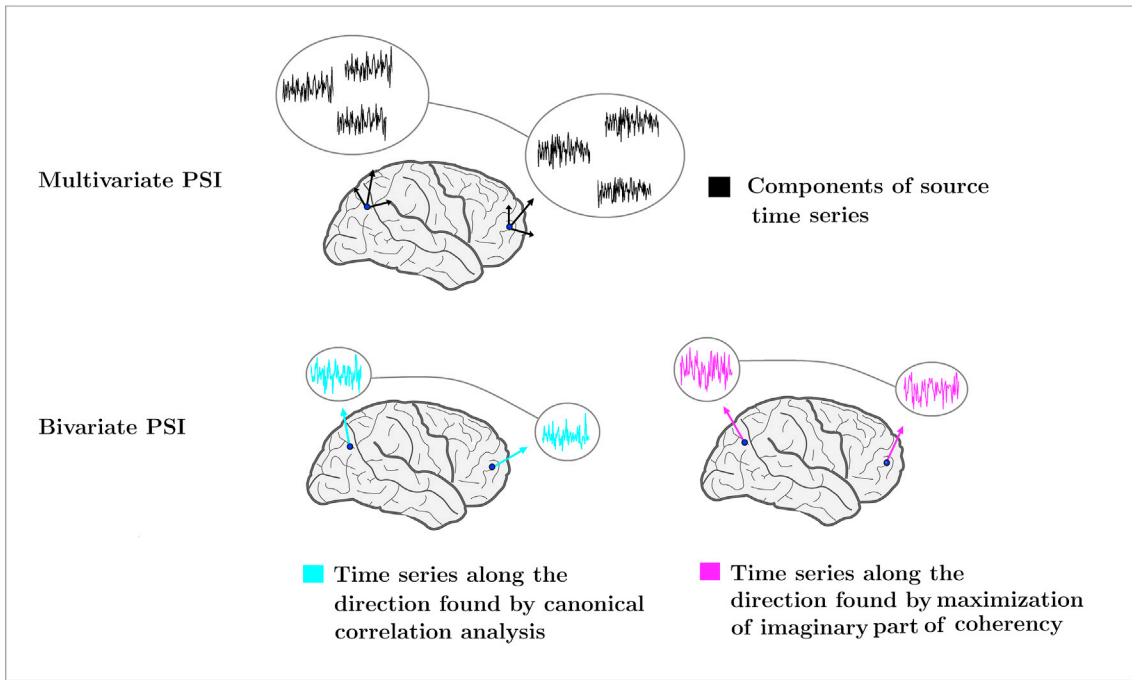
Fig. 1. Graphical representations of the multivariate (MPSI) and bivariate PSI. In particular, MPSI is able to directly assess directionalities from multivariate signals, e.g., from the time series of three-dimensional dipole moments at two brain locations, while the bivariate methods estimate directionality from two one-dimensional time series.

As for the bivariate PSI (Nolte et al., 2008, 2010), to assess the statistical significance of the observed results, it is convenient to consider a standardized version of MPSI. Indeed, by interpreting the ratio between MPSI and its standard deviation as a pseudo-*Z* score, and by fixing a level of significance, it is possible to read the observed *p*-values according to a Gaussian distribution. A complete description of an approach to estimate the standard deviation is provided in subsection 3.1.

Experiments

In this section, the experiments performed in this work are described. In the simulated studies, we evaluated the performance of MPSI in detecting the directionality of frequency-specific multivariate coupling in different synthetic experiments. Next, we assessed seed-based directed functional connectivity for resting state MEG data from the HCP database. The results obtained by MPSI in both simulated and real data were compared to the results obtained by two bivariate PSI approaches, i.e. PSI after the maximization of the imaginary part of coherency (MICPSI), and the PSI after canonical correlation analysis (CCAPSI).

Synthetic experiment 1

Here, we evaluate the performance of MPSI in assessing directionality from synthetic datasets consisting in pairs of multivariate time courses defined as a weighted superposition of a signal term, which represents a directed interaction between two vector sources of dimensions N_A and N_B, with a correlated noise term. This situation corresponds to an ideal case in which e.g. brain activity is a priori known without the need to estimate it from sensor level data. The case of estimated brain activity will be considered in the next section (Synthetic experiment 2).

Each simulated pair of multivariate time series Z_A and Z_B is combined in $Z = [Z_A^t \quad Z_B^t]^t$ and defined as

$$Z = (1 - \gamma) \frac{X}{||\mathbf{X}||_F} + \gamma \frac{Y}{||\mathbf{Y}||_F}, \tag{11}$$

where $X = [X_A^t \quad X_B^t]^t$ is the signal of interest, Y is a noise vector, $||\mathbf{X}||_F$

and $||\mathbf{Y}||_F$ are the Frobenius matrix norms of $\mathbf{X} = (X(1), ..., X(T))$ and $\mathbf{Y} = (Y(1), ..., Y(T))$. The value of $\gamma \in [0, 1]$ indicates the noise strength, thus e.g. $\gamma = 1/2$ indicates a balanced contribution between signal and noise for Z.

The time series of the leading source, which without loss of generality we assume to be A, $X_A = (x_1, ..., x_{N_A})^t$ and the evolution of the following source $X_B = (x_{N_A+1}, ..., x_{N_A+N_B})^t$ are defined as

$$x_i(t) = \sum_{j=1}^{N_A} \sum_{k=1}^{P} a_{ijk} x_j(t - \tau_k) + \xi_i(t), \quad i = 1, ..., N_A$$

$$x_i(t) = \sum_{j=N_A+1}^{N_A+N_B} \sum_{k=1}^{P} b_{ijk} x_j(t - \tau_k) + \sum_{j=1}^{N_A} \sum_{k=1}^{P} c_{ijk} x_j(t - \tau_k) + \xi_i(t),$$
$$i = N_A + 1, ..., N_A + N_B. \tag{12}$$

While the noise is modeled as

$$Y = (y_1, ..., y_{N_A+N_B})^t = M(\tilde{y}_1, ..., \tilde{v}_N)^t, \tag{13}$$

where the components, which are independent among them, have the following evolution

$$\tilde{y}_i(t) = \sum_{k=1}^{P} d_{ik} \tilde{y}_i(t - \tau_k) + \varepsilon_i(t) \quad i = 1, ..., N. \tag{14}$$

In equations (12) and (14) a_{ijk}, b_{ijk}, c_{ijk}, d_{ik}, $\xi_i(t)$ and $\varepsilon^i(t)$ are realizations of independent Gaussian random variables of zero mean and a standard deviation equal to $1/10$. Finally, $M \in \mathbf{R}^{(N_A+N_B) \times N}$ is a mixing matrix whose entries are realizations of a standard normal random variable.

For all the simulation repetitions, we set the dimension of each data space equal to 3, i.e. $N_A = N_B = 3$, the number of noise sources N equal to 6, the model order P equal to 5. Each of the generated time courses has a length of T = 76200 data points, which, sampled at 254 Hz, corresponds to 5 min of continuous data. With this approach, we used 20000 pairs of multivariate time series. Specifically, 2000 for each value of γ in the range from 0 (i.e., 100% signal) to 0.9 (i.e., 10% signal and 90 % noise) with an incremental step of 0.1. These 2000 pairs were further
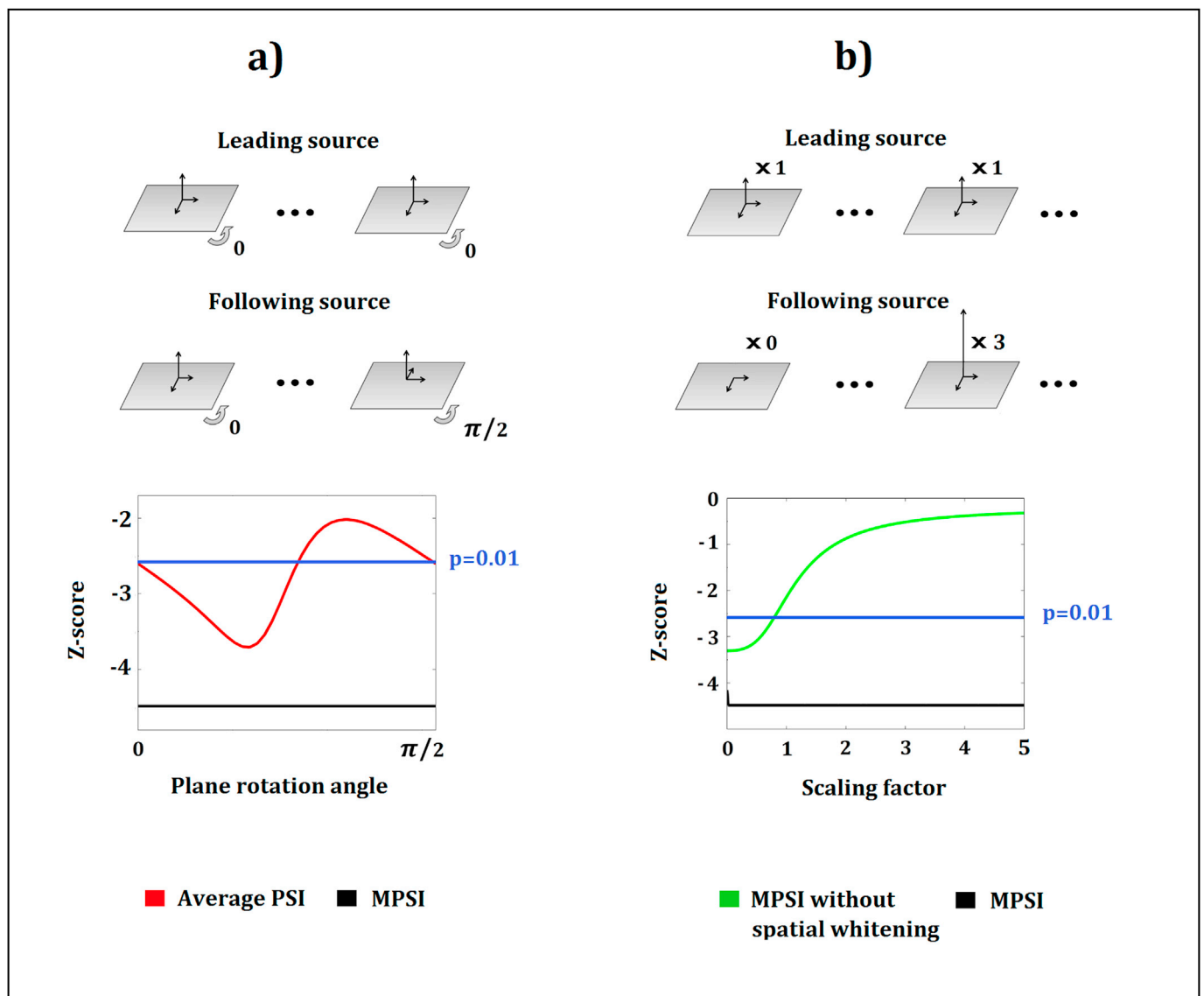
Fig. 2. A computational proof of the property of MPSI to be invariant under rotations and rescaling of signals, by using a simulated directed interaction between two three-dimensional sources. The panel a) shows the results obtained by MPSI and the average PSI, i.e. the bivariate PSI averaged over all the possible combination of scalar signals, when we applied rotations of the xy plane of one of the two vector signal. The panel b) shows the results of MPSI, with (i.e. as defined in (10)) and without the application of the spatial whitening (i.e. (10) but without the inverse matrices in the equation), as a function of a scaling factor.

divided into 20 sets of 100 pairs of time courses each, such that for each value of γ, the average percentage and standard deviation over the 20 sets of the number of right detections, of wrong detections and of no answers of MPSI in the alpha band (8–12 Hz) can be estimated.

The calculation of MPSI requires the estimation of the cross-spectra between time courses. To compute them, we firstly divided each multi-variate time series into $E = 150$ epochs of the same length, containing continuous data, and we further divided each epoch into 3 segments which have 50% overlap within each epoch but not across the epochs. We estimated the cross-spectra as an average of the products of the Fourier transforms over all segments (Nolte et al., 2008) and we calculated MPSI over each pair of frequencies f and $f + df$ for which at least one of them lies in the alpha band, by using a df value equal to 1 Hz.

To provide an estimation of the standard deviation (SD) of MPSI, we used the jackknife method (Nolte et al., 2008, 2010). In this approach, the SD of MPSI is defined over a set of its estimates, $MPSI^k$ with $k = 1, \ldots, E$, each obtained from the data in which the k-th epoch has been removed. The SD of the MPSI value is finally estimated for the E epochs as $\sqrt{E}\sigma$ where σ is the standard deviation of the set $\{MPSI^1, \ldots, MPSI^E\}$.

Finally, we used a significance level for the standardized MPSI equal to 0.01. This means that if the absolute value of MPSI for a given pair of time series exceeded 2.58, the direction of coupling detected by the sign of MPSI was considered as significant.

Synthetic experiment 2

Here, in order to investigate the impact of the MEG forward and inverse models on MPSI and the other phase slope based metrics, we performed biologically realistic simulations. Specifically, we simulated networks of interacting sources with two different levels of complexity. In the first case, we generated a single pair of interacting sources and four independent noise sources. In the second case, we simulated more complex networks, comprising four interacting sources and four independent noise sources, with a partially connected topology consisting of a directed closed cycle of three sources and a feed-forward connection from one of them to the fourth source.

The simulated time series at the level of brain regions were always modeled as single three-dimensional current dipoles with a temporal

evolution following equations in (12) for the drivers and the receivers. The evolution of the independent noise sources follows the same equation of the drivers, but without any source which receives information from them. For the simulation of the first case, the cortical locations of the two interacting regions were chosen to be located on the somatosensory areas (panel a) of Fig. 4 while, for each time series realization of the second case, the location of the four regions belonging to the simulated network were randomly chosen among six locations placed on parietal, frontal and temporal lobes (Fig. 5a). Finally, the noise sources for each different simulation realization were randomly located over the cortex.

In both cases, the simulated signals were projected to the sensor space to obtain the MEG recordings S as

$$S = (1 - \gamma) \frac{\sum_{i=1}^{N} L_i X_i}{\|\mathbf{X}\|_F} + \gamma \frac{\sum_{i=N+1}^{N+4} L_i Y_i}{\|\mathbf{Y}\|_F} + \mu, \tag{15}$$

where X and Y denote the time courses of the N interacting regions (two for the first case and four for the second case) and the four independent regions, γ denotes the strength of the biological noise, L is the spread pattern (i.e. leadfield matrix) for the neural sources and μ is an uncorrelated sensor noise with 0 mean and standard deviation equal to $1/10$. For each of the ten γ values considered (from 0 to 0.9 with step of 0.1), we generated 2000 time series. The length of each time series generated was 76200 data points which, with a sampling frequency of 254 Hz, corresponds to 5 min of continuously recorded activity. The leadfield matrix L was obtained by a single shell approach (Nolte, 2003) for one among the realistic source space, which consisted of a cortical layer of 8004 uniformly distributed points, and volume conductor model provided by the HCP.

Finally, in order to reconstruct the brain activities Z from S, we applied an inverse operator to generated MEG recordings. To this end, we used the eLoreta inverse method (Pascual-Marqui et al., 2011), a non-adaptive linear inverse solver with a weight matrix such that the estimated source distribution has maximal power at the true single dipole location. We relied on the eLoreta implementation provided in the FieldTrip toolbox (Oostenveld et al., 2011) where the weight matrix is obtained from the normalized leadfields. The cross-spectra in the alpha band (8–12 Hz) were estimated as averages of the products of the Fourier transforms over all segments and the SD of MPSI was estimated by using the jackknife method, as for the simulation described in the previous paragraph. Each directionality obtained from one of the methods was considered as significant if the absolute value of the measure was larger than 2.58, i.e. we used for all the methods a level of significance of 0.01.

In the first case, we assessed the mean value and the standard deviation of the number of right, wrong and not significant detections. In the second case, we assessed the ability to identify the correct topology of the simulated network by using a compound measure of pairwise coupling between all the different network nodes. Specifically, for each γ value, we computed the ratio between the mean squared errors (MSEs) in estimating the directionality of each simulated coupling. By denoting with $\omega_i \in \{-1, 1\}$ the parameter which describes if the direction of the $i-$ th simulated interaction is from source1 to source2 (source1-to-source2, $\omega = 1$), or from source2 to source1 (source2-to-source1, $\omega = -1$), we have that the MSE of MPSI in approximating $\Omega = \{\omega_i\}$ is defined as

$$\text{MSE(MPSI)} = \frac{1}{\#\text{time series pairs}} \sum_i (\text{sgn(MPSI}(i)) - \omega_i)^2, \tag{16}$$

where sgn (MPSI(i)) is equal to ± 1 if a statistical significant source1-to-source2 or source2-to-source1 direction for the $i-$ th coupling is detected by MPSI, while, it is equal to 0 if the detected directionality is considered to be not statistically significant. Analogously, MSEs for MICPSI and CCAPSI can be defined. The ratio between the MSE of MPSI and the MSE of either MICPSI or CCAPSI allows a direct comparison between the performance MPSI and the other two approaches. Hence, a value lower than 1 for this ratio implies a better performance of MPSI in disclosing statistically significant directionalities, while a value larger than 1 implies the opposite. To calculate the average and standard deviation of the number of right detections, of wrong detections, of not significant detections and of MSEs of the three methods, the generated signals were divided into 20 sets of 100 pairs.

Real MEG data experiment

Resting state MEG data from Human Connectome Project

Resting-state MEG data were taken from 61 subjects as part the HCP MEG2 release (Larson-Prior et al., 2013). The release included a total of 67 subjects, but resting-state recordings that passed the quality control checks were not available from 6 of them, leading to the final cohort of 61 subjects, all young (22–35 years of age) and healthy. The same cohort of 61 subjects was used in Colclough et al. (2016). For each subject, resting-state data were measured using a whole-head Magnes 3600 scanner (4D Neuroimaging, San Diego, CA, USA) in three consecutive sessions lasting 6 min each. Preprocessing, as provided in the MEG2 release, included: data down-sampling to 508.6 Hz, removal of noisy time segments from the recordings, identification of faulty recording channels, and artefact rejection based on an independent component
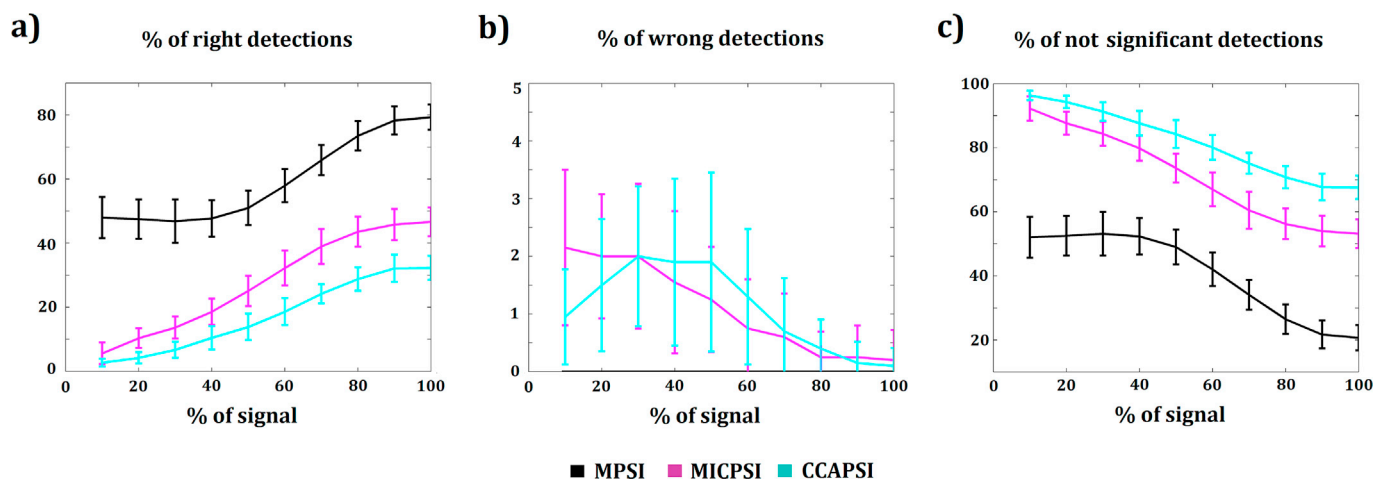

Fig. 3. Average percentages and standard deviations of a) right, b) wrong and c) not significant detections are shown for the three methods, i.e. multivariate PSI (MPSI), the bivariate PSI with a maximization of imaginary part of coherency approach (MICPSI) and the bivariate PSI with a canonical correlation analysis approach (CCAPSI).
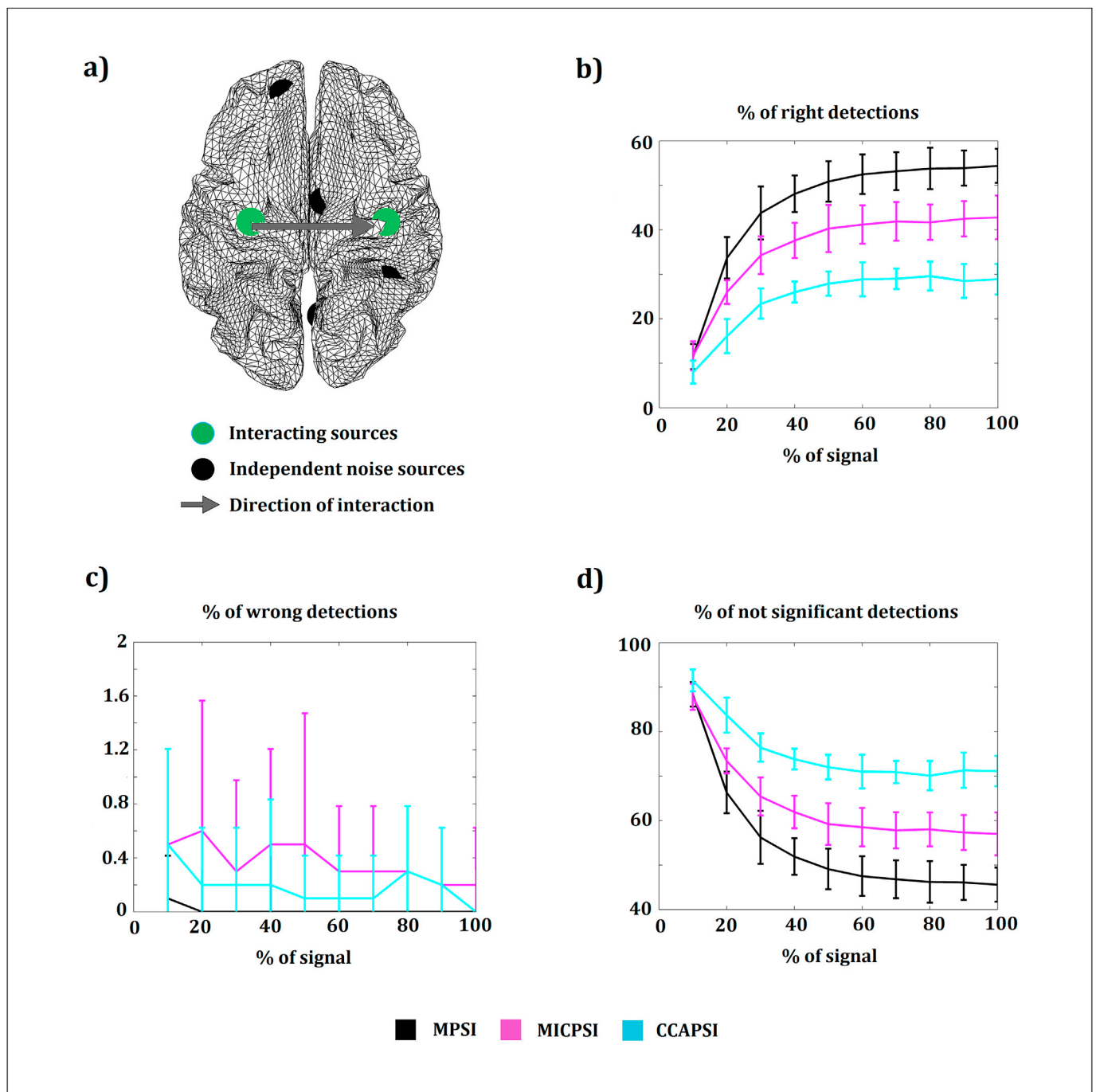
Fig. 4. The panel a) shows the locations of the interacting sources (green dots), with the direction of the interaction, and the locations of the independent noise sources (black dots) for a single time series realization. The panels b), c) and d) show, respectively, the average percentages and standard deviations of right, wrong and not significant detections for the three methods.

analysis (ICA) decomposition (Mantini et al., 2011). For ease of computation, we further down-sampled the data to 254.3 Hz.

A seed-based analysis was used to assess functional connectivity in the alpha band. As a preliminary step, we applied a data driven approach based on power maps in the alpha frequency band to identify the seed location as the location of maximum alpha power.

To this end, we computed channel level power from each session in the alpha band using a set of 7 orthogonal Slepian tapers (Slepian, 1978) with a 10 Hz center frequency to produce 2 Hz frequency smoothing. Alpha band power in source space, which consisted of a cortical layer of 8004 uniformly distributed points, was estimated by the eLoreta inverse procedure with free source orientation (Pascual-Marqui et al., 2011). We

relied on the eLoreta implementation provided in the FieldTrip toolbox (Oostenveld et al., 2011) where the weight matrix is obtained from the normalized lead fields obtained with the single shell approach (Nolte, 2003) for the source space and volume conductor model provided by the HCP. The group averaged alpha power map was obtained as the mean across all sessions and subjects. The HCP source space and volume conductor model are already provided in the standard co-ordinate space of the Montreal Neuroimaging Institute (MNI), thus allowing straightforward group averaging. Finally, the seed was defined as the location corresponding to maximum alpha power.

Once the seed location has been identified as above, seed-based MPSI analysis in source space has been performed and the directed connec-
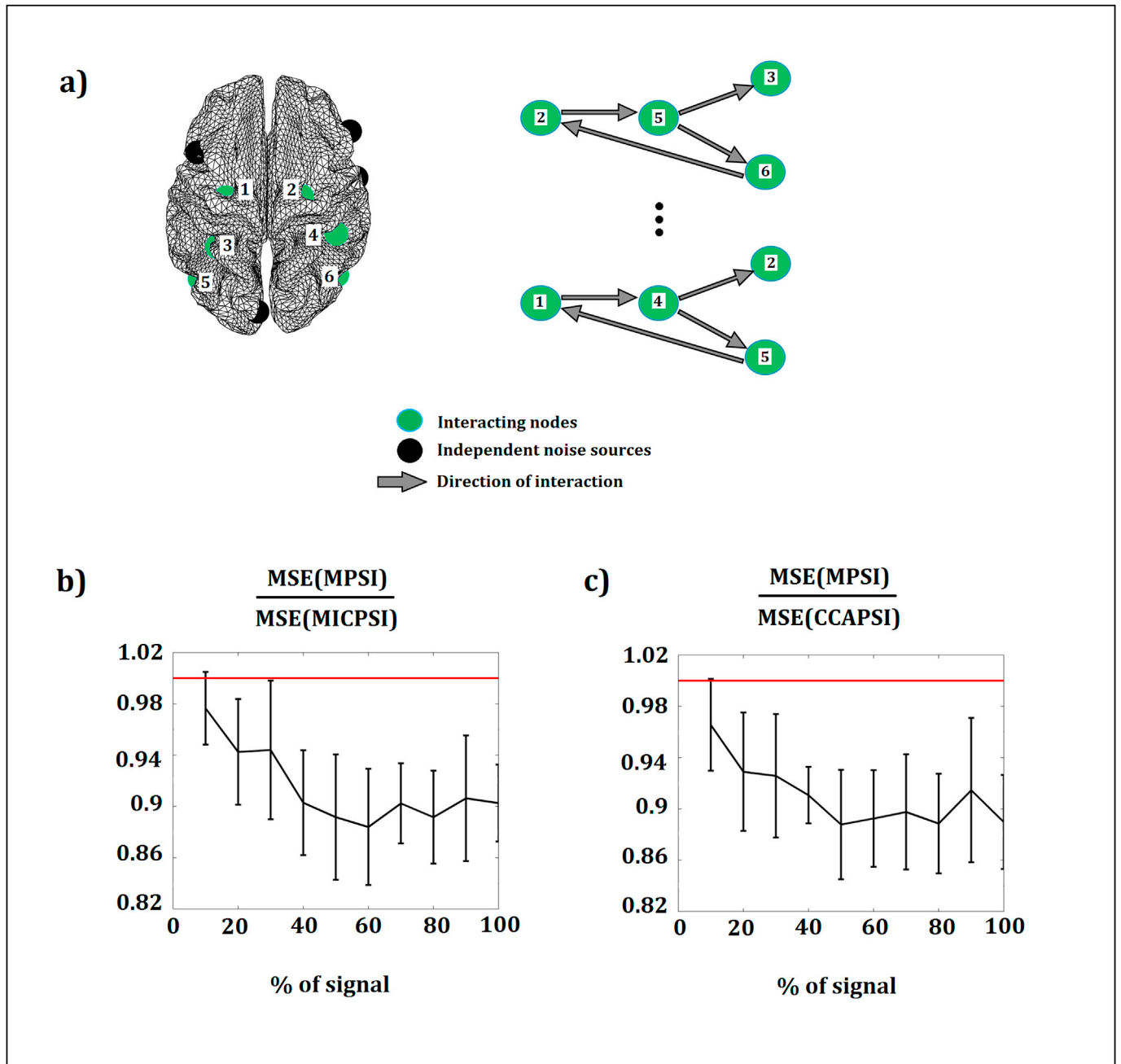
Fig. 5. a) The possible locations for the four interacting sources, their role in the simulated network by varying the realization simulations and a possible location for the four independent sources. The ratio between b) the mean square error (MSE) of MPSI and the MSE of MICPSI and between c) the MSE of MPSI and the MSE of CCAPSI.

tivity map has been obtained as the map of

$$\mathrm{MPSI}_{A,B} = \frac{1}{\sqrt{3 \cdot 61}} \sum_{ses=1}^{3} \sum_{sub=1}^{61} \frac{\mathrm{MPSI}_{A,B}^{ses,sub}}{std\left(\mathrm{MPSI}_{A,B}^{ses,sub}\right)}, \qquad (17)$$

where $1/\sqrt{3 \cdot 61}$ is a normalization factor used to have the standard deviation of the group MPSI equal to 1. In other words, the map was obtained as the average over the 61 subjects and the 3 sessions of the standardized MPSI between the multidimensional source time series of any cortex location A and the multidimensional source time series of the seed, denoted by B.

The estimates of the cross-spectra and of the SDs of MPSI were computed as for the synthetic data. Furthermore, we used the same level of significance, i.e. we considered as statistically significant only

observed $p < 0.01$. Nevertheless, to account for multiple comparisons, a false discovery rate (FDR) correction on the observed p-values has been used.

Bivariate approaches based on PSI

The results obtained from MPSI on synthetic and measured time series were compared to the results of other two methods based on the phase slope, namely MICPSI and CCAPSI.

More specifically, MICPSI is the bivariate PSI between two scalar time series obtained from an approach based on the maximization of the imaginary part of coherency (Ewald et al., 2012) applied to the multivariate signals Z_A and Z_B, i.e. the PSI between the bivariate signals $\tilde{\alpha}^t Z_A$

and $\tilde{\beta}^t Z_B$ where

$$
\begin{aligned}
\tilde{\alpha} &:= \text{argmax}_{||\alpha||=1} \left\{ \alpha^t \sum_{f \in F} \left(S_{AA}^R(f)^{-\frac{1}{2}} S_{AB}^I(f) S_{BB}^R(f)^{-1} S_{BA}^I(f) S_{AA}^R(f)^{-\frac{1}{2}} \right) \alpha \right\} \\
\tilde{\beta} &:= \text{argmax}_{||\beta||=1} \left\{ \beta^t \sum_{f \in F} \left(S_{BB}^R(f)^{-\frac{1}{2}} S_{BA}^I(f) S_{AA}^R(f)^{-1} S_{AB}^I(f) S_{BB}^R(f)^{-\frac{1}{2}} \right) \beta \right\}.
\end{aligned} \tag{18}
$$

In (18) S_{AA}, S_{BB}, S_{AB} and S_{BA} indicate cross-spectral matrices, and the superscripts R and I denote the real and imaginary part, respectively, following the same notation adopted in equation (4). Hence the directions, $\tilde{\alpha}$ and $\tilde{\beta}$, over which the multivariate signals are projected are those which allow for the maximization of the imaginary part of the coherency between any pair of bivariate signals $\alpha^t Z_A$ and $\beta^t Z_B$ in the alpha band.

On the other hand, CCAPSI is a bivariate PSI between two scalar time series obtained from canonical correlation analysis (Hotelling, 1936) as detailed below. Let us define the alpha band-filtered data $\tilde{Z}_A$ and $\tilde{Z}_B$ obtained from the original signals Z_A and Z_B. The estimator of directionality is then the bivariate PSI between the time series $\tilde{\alpha}^t Z_A$ and $\tilde{\beta}^t Z_B$ where the vectors $\tilde{\alpha}$ and $\tilde{\beta}$ are defined as:

$$
\begin{aligned}
\tilde{\alpha} &:= \text{argmax}_{||\alpha||=1} \left\{ \alpha^t (\Sigma_{AA})^{-\frac{1}{2}} \Sigma_{AB} (\Sigma_{BB})^{-1} \Sigma_{BA} (\Sigma_{AA})^{-\frac{1}{2}} \alpha \right\} \\
\tilde{\beta} &:= \text{argmax}_{||\beta||=1} \left\{ \beta^t (\Sigma_{BB})^{-\frac{1}{2}} \Sigma_{BA} (\Sigma_{AA})^{-1} \Sigma_{AB} (\Sigma_{BB})^{-\frac{1}{2}} \beta \right\}
\end{aligned} \tag{19}
$$

where Σ_{AB} denotes the covariance between $\tilde{Z}_A$ and $\tilde{Z}_B$, and similarly for Σ_{BA}, Σ_{AA}, and Σ_{BB}. Thus, the bivariate PSI is calculated on the directions, $\tilde{\alpha}$ and $\tilde{\beta}$, which allow for a maximization of the temporal correlation between any pair of bivariate signals $\alpha^t \tilde{Z}_A$ and $\beta^t \tilde{Z}_B$.

The approaches used to estimate the cross-spectra between time courses, which are the basis for MICPSI and CCAPSI computation, as well as for SDs, are the same described in subsection 3.1.

Results

Synthetic experiment 1

We found that MPSI outperforms both PSI based methods, i.e. MICPSI and CCAPSI, as shown in Fig. 3a. Indeed, MPSI features a percentage of right detections which is two to four times (in case of high or low signal percentage, respectively) the corresponding percentages featured by MICPSI and CCAPSI. Conversely, no substantial differences among the three methods in the number of wrong detections are evident (Fig. 3b). Actually, all estimators have obtained very low average percentages of wrong detections ($< 3\%$), even in very noisy conditions, showing the robustness to noise of both the multivariate and the bivariate phase slope based methods. However, it is important to notice that, over all the simulation realizations, the number of pairs in which MPSI has detected a wrong directionality is exactly 0. Finally, Fig. 3c shows the percentage of not statistically significant detections for the three methods. Specifically, the percentage for MPSI decreases as the signal percentage increases reaching a value of about 20%. Conversely, the curves for MICPSI and CCAPSI, clearly show a slower decrease with average percentages always larger than 50%. Thus, the observed prominent difference between MPSI and the two bivariate methods is basically due to the large number of multivariate pairs for which MICPSI and CCAPSI are not able to asses a statistically significant directionality.

Synthetic experiment 2

When the effect of the MEG forward/inverse model and of biological noise are taken into account, a consistent difference in the performance between MSPI and the bivariate estimators is also evident. In the simple case, with a network made by only two nodes, the results are shown in

Fig. 4 panels b), c), d). Specifically, MPSI achieves the highest number of right detections, panel b), and the lowest number of not significant detections and wrong detections, panels c) and d), in comparison to both MICPSI and CCAPSI. This general behaviour is in accordance with the results found for the "Synthetic experiment 1" in which the effect of MEG forward/inverse model was not considered.

The results obtained for the complex network case are shown in Fig. 5 and Fig. S1 of the Supplementary Material. Here, we compared the mean squared errors (MSEs) of the different methods in reconstructing the correct topology of the simulated network. The ratio between the MSE of MPSI and the MSEs of the other two methods, panel b) for MCIPSI and panel c) for CCAPSI, is always lower than 1. Moreover, the MSE of MPSI is, on average, about 10% lower than each of the other two MSEs. This result thus reveals that MPSI is, for every noise condition, better at reconstructing the topology of the simulated network.

Real MEG data experiment

For the HCP resting state MEG data, the cortical location associated with the maximum of the group averaged alpha power was used as seed for the directed functional connectivity analysis (Fig. S2 panel A). The resulting location belongs to the "calcarine fissure" parcel of the AAL Atlas (Tzourio-Mazoyer et al., 2002) and specifically it is positioned in the right primary visual cortex (V1) at MNI coordinates (6.5, -62.5, 18.5) mm (grey dot on the right medial view in Fig. 6, Fig. 7, Fig. S2 and Fig. S3).

Fig. 6 shows the FDR corrected ($p < 0.01$) group averaged map in the alpha band between V1 and all other locations over the cortex obtained by applying MPSI.

In this map, regions which exert an influence on V1 are color coded in red while regions on which V1 exerts an influence are indicated in blue. Specifically, we observe as a prominent feature an input from V1 to occipital cortex, left and right frontal cortex, and medial prefrontal cortex. Conversely, bilateral parietal areas and the posterior cingulate cortex lead V1.

Of note, all of the above areas belong to well-known resting state networks (RSNs), i.e. sets of brain regions exhibiting temporally correlated activity fluctuations in the absence of imposed task structure ((Deco and Corbetta, 2011), (Fox et al., 2005), (Smith et al., 2009)). Indeed, the MPSI map in Fig. 6 shows that areas of dorsal attention network (DAN), fronto-parietal network (FPN), ventral attention network (VAN), default mode network (DMN) and visual network (VN) are coupled to V1 in the alpha band. Specifically: i) for DAN areas, an influence on V1 is exerted by the left and right superior parietal lobule (SPL); ii) for FPN areas, while the left inferior parietal sulcus (IPS) and the right inferior parietal lobule (IPL) lead V1, the left dorsolateral prefrontal cortex (dlPFC) follows V1; iii) for VAN areas, the right inferior frontal gyrus (IFG) and the right anterior insula (AI) are influenced by V1; iv) for DMN areas, the posterior cingulate cortex (PCC) exerts an influence on V1 while V1 leads the medial prefrontal cortex (mPFC); v) for VN areas, left primary visual areas. RSN nodes, whose MNI coordinates are listed in Table 1, are taken from Hacker et al. (2013) and Marzetti et al., 2013.

These MPSI results can be compared to the results on the same data and frequency band obtained by the bivariate PSI approaches. Indeed, Fig. 7 shows a comparison of the MPSI results with MICPSI and CCAPSI results (FDR corrected $p < 0.01$). Although some of the observed directed interactions with V1 are visible for all metrics, e.g. an input from V1 to the right occipital cortex and from parietal areas to V1, differences in group averaged functional connectivity maps are evident. Specifically, CCAPSI in contrast to MPSI did not detect a statistically significant input from V1 to the right middle frontal cortex and left inferior frontal cortex, while MICPSI detected these couplings only to a lower extent. Furthermore, MPSI is the only method among the three which is able to disclose an input from V1 to the right and left mPFCs and from PCC to V1.

Altogether, the maps obtained by applying the bivariate methods on real MEG data show fewer regions which exhibit directed interactions
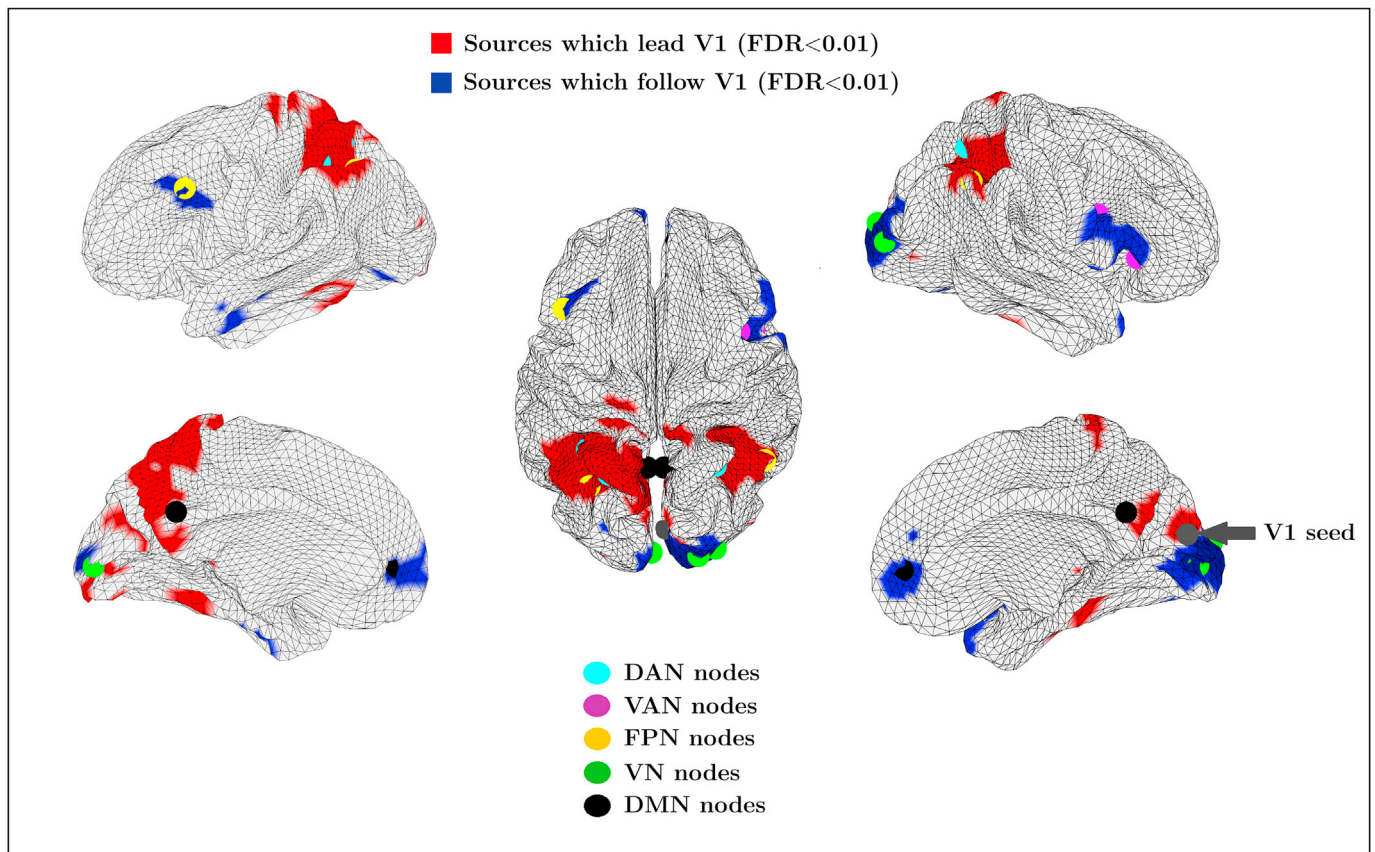
Fig. 6. The FDR corrected (*p* <0.01) group averaged map in the alpha band between V1 (grey dot on the right medial view) and all other locations over the cortex obtained by using MPSI approach is shown. Red cortical locations exert an influence on V1 while V1 exerts an influence on blue coloured regions. The coloured dots represent resting state network nodes which overlap the blue and red areas.

with V1 with respect to the map obtained by using MPSI.

Finally, a point-to-point comparison between the group averaged alpha power map and the group averaged MPSI map results into a very small value of the square of Pearson correlation between MPSI and the alpha power value ($r^2 = 0.047$) indicating a weak degree of predictability between the two variables. Specifically, only the 4.7% of the variation of the MPSI values can be explained by the variation in the alpha power (Fig. S2).

Discussion

In this work, we developed and successfully applied to synthetic and real data, the multivariate phase slope index (MPSI), a generalization to multivariate time series of the phase slope index (PSI) (Nolte et al., 2008) directed connectivity method, that retains the desirable property of being by construction robust to the artificial brain source coupling. MPSI is able to disclose the directionality of frequency-specific neural interactions from multivariate electrophysiological signals, such as those associated to the brain sources as reconstructed from magnetoencephalographic (MEG) or electroencephalographic (EEG) data. The usual way to detect directionality of frequency-specific neural interactions from e.g. MEG source time courses is to first find, for each source, a scalar time series obtained by a priori fixing the source orientation, and second to use a bivariate approach on the reduced time series of the sources. Conversely, MPSI can directly assess the coupling direction from e.g. MEG source time courses, without fixing an a priori orientation.

The results obtained on simulated data prove that MPSI achieves substantial higher performance than bivariate PSI approaches in detecting directionality of multivariate interactions, i.e. with source orientation fixed according to a canonical correlation based approach and with

source orientation fixed according to the maximization of imaginary coherency. Indeed, the latter procedures lead to unavoidably discard part of the signal and to not completely exploit the multivariate nature of the sources, thus supporting the notion that bivariate estimators perform worse than multivariate methods (Marzetti et al., 2013). Additionally, biologically realistic simulations have proven that MPSI outperforms the other two tested approaches also when the sources are considered as resulting from the solution of an MEG inverse approach. This is true for the estimation of directionality between two sources in a simple network, but also for the detection of the topology of a more complex network with several interacting and non-interacting nodes and with a given pattern of directionality among the interacting sources. Importantly, the general pattern of these results is only mildly affected by the simulated signal strength, indicating that MPSI is able to correctly assess the directionality also for signals with low signal-to-noise ratio.

MPSI has also proven to be able to disclose directed interactions in real MEG data from a resting state experiment in 61 subjects from the Human Connectome Project database. Our findings are in line with the existing MEG observations of resting state alpha band coupling between the Visual Network and other RSNs (Brookes et al., 2011; de Pasquale et al., 2010, 2012; Marzetti et al., 2013). In addition, our study provides an insight into a directed coupling between the visual cortex and DAN, VAN and FPN which is in accordance with feedback and feedforward relations (Varela et al., 2001) between areas of these networks (Vossel et al., 2014; Corbetta and Shulman, 2002). Specifically, the results concerning the coupling from the DAN to the visual cortex are in accordance with the idea of a feedback control exerted by the DAN on visual areas to instantiate goal-directed control of attention (Corbetta and Shulman, 2002). Along the same line, the observed coupling from the visual cortex to the VAN can be attributed to the role of the VAN in stimulus driven
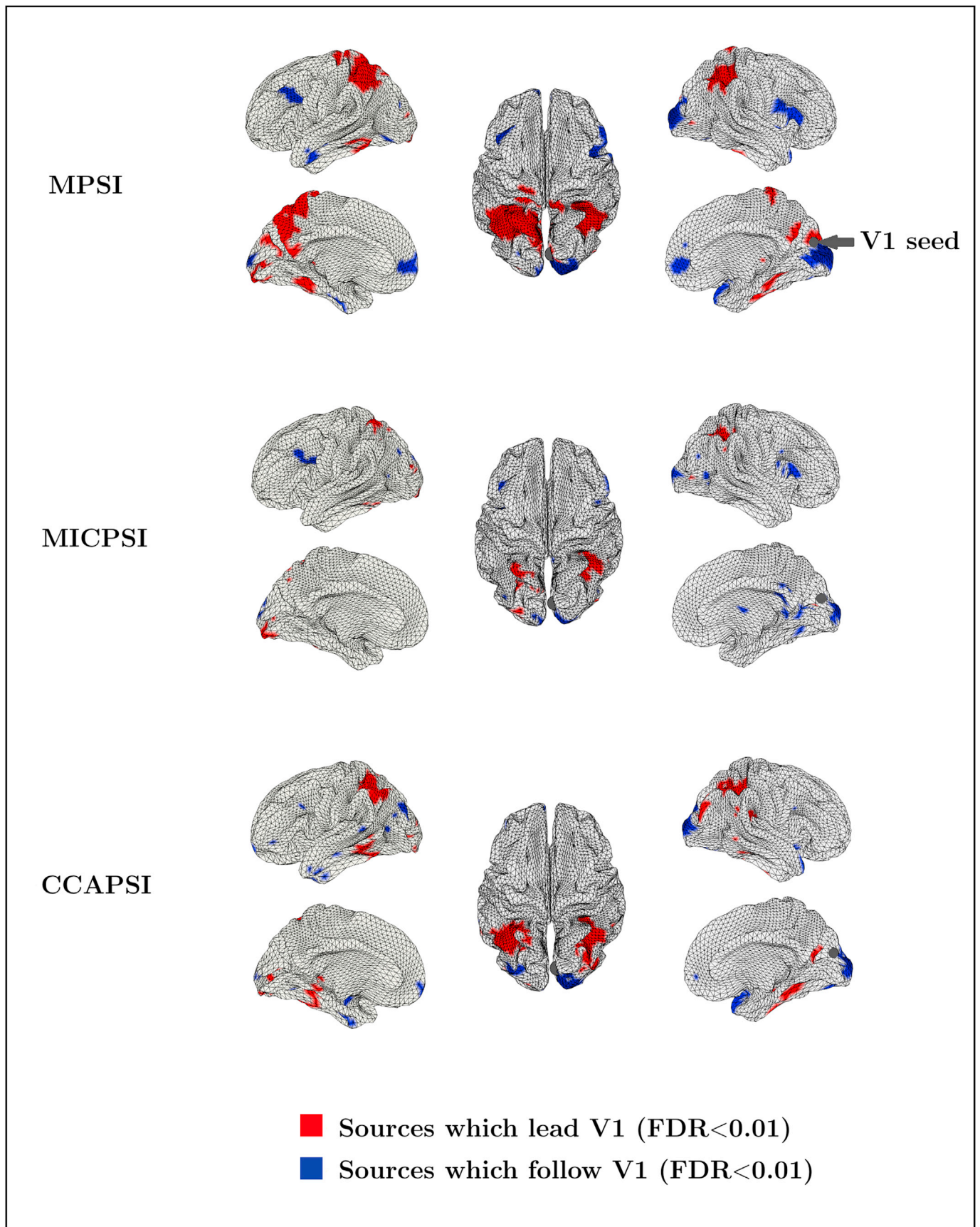
Fig. 7. The FDR corrected ($p < 0.01$) group average MPSI, MICPSI and CCAPSI maps of the directed functional connectivity in the alpha band for the 61 HCP MEG subjects are shown.

Table 1

Resting State Network nodes, their MNI coordinates (mm) and the directionality of their interactions with V1 seed revealed by using MPSI. A leading role exerted on V1 is denoted with the symbol → while, a following role, with the symbol ←.

Cortical area	MNI coord. (x, y, z)	Direction	Resting State Network
left aIPS	(−32.3, −45.6, 46.6)	→ V1	Dorsal Attention Network
left SPL	(−22.2, −57.3, 53.6)	→ V1	Dorsal Attention Network
right SPL	(28.3, −53.1, 53.8)	→ V1	Dorsal Attention Network
left dlPFC	(−43.4, 20.9, 38.1)	← V1	Fronto-Parietal Network
left IPL	(−31.3, −62.9, 42.4)	→ V1	Fronto-Parietal Network
right IPL	(51.5, −50.6, 43.0)	→ V1	Fronto-Parietal Network
right vPrCe	(39.4, 10.2, 23.4)	← V1	Ventral Attention Network
right IFG-AI	(42.4, 28.8, 2.6)	← V1	Ventral Attention Network
right vIFG	(46.5, 10.9, 10.4)	← V1	Ventral Attention Network
left PCC	(−4.0, −54.0, 30.0)	→ V1	Default Mode Network
left mPFC	(−10.0, −53.0, 2.0)	← V1	Default Mode Network
right PCC	(4.0, −54.0, 30.0)	→ V1	Default Mode Network
right mPFC	(10.0, 53.0, 2.0)	← V1	Default Mode Network
left dV2	(−2.0, −94.1, 3.7)	← V1	Visual Network
right V3	(20.2, −95.7, 14.5)	← V1	Visual Network

control of attention (Corbetta and Shulman, 2002). We also found a twofold coupling between the visual cortex and the FPN. Indeed, while the parietal parts of the FPN exert a leading role on the visual cortex in line with the notion that FPN controls cognitive processes through a feedback mechanism (Dosenbach et al., 2008), the dlPFC is connected to the visual cortex in a feedforward fashion. The latter result is in accordance with the putative role of this region in action preparation in response to the visual stimulus (Heekeren et al., 2006).

The observed coupling between the visual network and the DMN can be ascribed to the processing of internal visual representations related to the DMN. Indeed, our directionality results are in line with the hypothesis that PCC, which is known to be involved in visual imagery (Cavanna and Trimble, 2006), exerts a control on the visual cortex to instantiate a visual response even in the absence of a visual stimulus (Tong, 2004), and that, in turn, the visual cortex sends inputs to the mPFC node of the DMN which is known to be involved in mentalizing and self-referential processing (de Pasquale and Marzetti, 2014; Marzetti et al., 2014). Finally, the internal coupling observed within the visual network is consistent with previous observations that primary visual areas lead secondary and associative visual areas according to a feedforward model (Riesenhuber and Poggio, 1999) to account for, e.g., the ability to recognize specific objects.

In conclusion, the relatively large cohort of subjects from the Human Connectome Project allowed us to conclude that the alpha band directed interactions between visual cortex and several RSNs are a remarkable feature of MEG resting state networks coupling. An interesting perspective for future studies would be the reproducibility of this feature in single subjects as well as its alterations in brain diseases.

As for the simulated situations, the differences in the directed functional connectivity results for the three methods observed in real data are likely to be attributed to the higher performance of the MPSI in the detection of the coupling direction between areas which conceivably have a multivariate nature. Indeed, in the simulation studies we found a large number of multivariate couplings in which, as opposed to MPSI, MICPSI and CCAPSI did not succeed to disclose a statistically significant directionality. The unthresholded resting state maps reveal that the same behaviour holds for the three methods at different significance levels. Thus, ultimately suggesting that MPSI is able to detect the same coupling directions of MICPSI and CCAPSI but with noisier data, e.g. with lower number of subjects.

An additional interesting general issue to be discussed when connectivity is the target is to what extent the connectivity maps differ from the power maps. We have thus investigated, in the real data experiment, if there is a direct relation between the group averaged MPSI maps (with respect to the primary visual cortex) and the corresponding alpha band

power maps. Our results have shown a weak degree of predictability between the power and MPSI on a point-to-point basis on the cortex. Moreover, the points corresponding to cortical regions belonging to the tail of the 5% of sources with the highest power can have either small or large, positive or negative, in the corresponding MPSI map (Fig. S2). This result is conceivable given that MPSI implies a whitening step which takes into account power normalization. Indeed, although this normalization is not able to exactly flatten at the same time the power at frequency f and at frequency $f + \mathrm{d}f$ from a theoretical point of view, in practice, given that power variations across frequency within physiological bands are smooth, this normalization results into making MPSI results not driven by power results.

Even though MPSI has extensively proven to be a better estimator of the directionality than the tested bivariate versions, one must be aware of a potential limitation of these approaches. Indeed, all phase slope based methods can detect the directionality of delayed interactions only and, thus, the direction of the functional couplings occurring at zero phase cannot be assessed by MPSI as well as by the bivariate PSIs. Nevertheless, it is unlikely that perfectly zero phase interactions occur in the brain consistently with the communication through coherence model (Fries, 2015) and as reasonable due to conduction delays in physical communication between brain areas.

Additionally, while in this work we compared only methods based on phase slope, other computational approaches which exploit different features of the data have been defined to assess the directionality of neural couplings. It will be thus interesting to investigate in future studies the performance of MPSI as compared to other types of measures, e.g. based on Granger causality (GC) (Geweke, 1982; Granger, 1969). Of note, GC based approaches do not differ from phase based approaches in that they also assess directionality by relying on temporally delayed signals. Moreover, most of GC based measures are not able to cope with the negative effects of field spread, and the use of an orthogonalization procedure (Brookes et al., 2012; ONeill et al., 2015) prior to their application can indirectly make the obtained results robust to these effects. For example, a bivariate GC approach in the frequency domain (Geweke, 1982) can be used to assess directionality from synthetic scalar signals obtained by maximizing the power of the two simulated sources after orthogonalization. Preliminary simulations referring to data generated with the Synthetic experiment 1 approach (Fig. S4) show that also in this case the use of a bivariate approach on multivariate data results in a lower percentage of right detections. Indeed, several GC versions exist, e.g.: the one in the time domain (Granger, 1969), the nonlinear one (Marinazzo et al., 2008), or other slightly different measures such as the partial directed coherence (Baccalá and Sameshima, 2001) or the directed transfer function (Blinowska et al., 2004). An extensive comparison between phase slope based methods and these Grager causality versions is beyond the scope of this work and will be the topic of future investigations.

Finally, while the real data results have provided interesting insights into RSNs directed interactions, a whole brain all-to-all connectome in which directionality between all brain areas is assessed would provide a broader view on brain functioning. Therefore, while a connectomic approach was beyond the scope of this work, we believe that an all-to-all approach is a worth direction to take in future works and that MPSI should be used to derive directed frequency specific all-to-all connectomes, which can be subsequently subject to e.g. graph analysis (Bullmore and Sporns, 2009; Rubinov and Sporns, 2010). In fact, being the MPSI defined as a product of cross-spectral matrices, a fast implementation of MPSI that allows to derive a dense functional connectome is indeed possible. Additionally, a connectomic approach would further limit the possible effects induced by spurious interactions from ghost sources on the observed results (Palva and Palva, 2012) with respect to seed based approaches.

Appendix A. Supplementary data

Supplementary data related to this article can be found at https://doi.org/10.1016/j.neuroimage.2018.03.004.

Appendix A. PSI and MPSI vanish for linear mixtures of independent sources

The purpose of this appendix is to show an explicit proof that PSI and MPSI are robust to the artificial and instantaneous coupling induced by field spread effects in source space.

Let us assume that the one-dimensional sensor signals $\{\sigma_i\}_{i=1}^{N_{\text{sensors}}}$ can be written as a superposition of N_{sources} three-dimensional brain sources, denoted by $\{(x_{1k}, x_{2k}, x_{3k})\}_{k=1}^{N_{\text{sources}}}$. Therefore, for a fixed channel i it holds that its Fourier transform can be written as $\widehat{\sigma}_i(f) = \sum_{g=1}^{3} \sum_{j=1}^{N_{\text{sources}}} L_{igj}\widehat{x}_{gj}(f)$, where $L \in \mathbf{R}^{N_{\text{sensors}} \times 3 \times N_{\text{sources}}}$ is the leadfield tensor and f is a fixed frequency. The application of an inverse procedure to the N_{sensors} signals leads to the definition of $\tilde{N}_{\text{sources}}$ reconstructed source time series $\{(z_{1k}, z_{2k}, z_{3k})\}_{k=1}^{\tilde{N}_{\text{sources}}}$. The h-th component of the k-th three-dimensional vector is thus described, in the frequency dependent domain, as $\widehat{z}_{hk}(f) = \sum_{i=1}^{N_{\text{sensors}}} W_{hki}\widehat{\sigma}_i(f)$, where $W \in \mathbf{R}^{3 \times \tilde{N}_{\text{sources}} \times N_{\text{sensors}}}$ is the inverse operator. Moreover, these reconstructed source time courses can be in turn expressed as a superposition of the components of the actual brain sources, as in:

$$\widehat{z}_{hk}(f) = \sum_{i=1}^{N_{\text{sensors}}} W_{hki}\widehat{\sigma}_i(f) = \sum_{i=1}^{N_{\text{sensors}}} \sum_{g=1}^{3} \sum_{j=1}^{N_{\text{sources}}} W_{hki}L_{igj}\widehat{x}_{gj}(f)$$
$$= \sum_{g=1}^{3} \sum_{j=1}^{N_{\text{sources}}} \widehat{x}_{gj}(f) \sum_{i=1}^{N_{\text{sensors}}} W_{hki}L_{igj} = \sum_{g=1}^{3} \sum_{j=1}^{N_{\text{sources}}} R_{hkgj}\widehat{x}_{gj}(f) \tag{20}$$

where $R \in \mathbf{R}^{3 \times \tilde{N}_{\text{sources}} \times 3 \times N_{\text{sources}}}$ is the resolution tensor.

As we previously noted, to apply the bivariate PSI on a pair of reconstructed source time courses it is necessary to fix a unidimensional time series for each vector source. To this end, a transformation that leads each three-dimensional source time series into a scalar time series has to be defined. Alternatively, it is possible to use MPSI which is basically an average process defined over the bivariate PSIs calculated between time series which are obtained by a suitable linear mixing of the components of the vector sources. Thus, to prove that PSI and MPSI are robust to the negative field spread effects, it is sufficient to show that the cross-spectrum between every pair of linear combination of the source components is a real number if the components of two different brain sources are non-interacting and the components of the same brain source have among them a zero-phase difference. Indeed, a real cross-spectrum would imply zero values for PSI and MPSI given that the PSI numerator at frequency f can be written as a difference between products of real and imaginary parts of cross-spectra as in: $\Im(s_{1,2}(f+\mathrm{d}f))\Re(s_{1,2}(f)) - \Im(s_{1,2}(f))\Re(s_{1,2}(f+\mathrm{d}f))$. Thus, if the imaginary part of cross-spectrum vanishes, it also vanishes PSI and MPSI.

We thus have to prove that the cross-spectrum between $\sum_{h=1}^{3} T_{hk}z_{hk}$ and $\sum_{e=1}^{3} T_{el}z_{el}$, where $T \in \mathbf{R}^{3 \times \tilde{N}_{\text{sources}}}$, is real for all k and l in the range $1, \dots, \tilde{N}_{sources}$. By using that the components of the reconstructed sources can be written as functions of the components of the actual brain sources and by using that R and T are not time dependent, it holds that

$$\left\langle \left(\sum_{h=1}^{3} T_{hk}\widehat{z}_{hk}\right)\left(\sum_{e=1}^{3} T_{el}\widehat{z}_{el}\right)^* \right\rangle = \sum_{h=1}^{3}\sum_{e=1}^{3} T_{hk}T_{el}\left\langle \widehat{z}_{hk}(f)\widehat{z}_{el}^*(f) \right\rangle = \sum_{h=1}^{3}\sum_{e=1}^{3} T_{hk}T_{el}\left\langle \left(\sum_{g=1}^{3}\sum_{j=1}^{N_{\text{sources}}} R_{hkgj}\widehat{x}_{gj}(f)\right)\left(\sum_{d=1}^{3}\sum_{i=1}^{N_{\text{sources}}} R_{eldi}\widehat{x}_{di}(f)\right)^* \right\rangle$$
$$= \sum_{h=1}^{3}\sum_{e=1}^{3} T_{hk}T_{el} \sum_{g=1}^{3}\sum_{d=1}^{3}\sum_{j=1}^{N_{\text{sources}}}\sum_{i=1}^{N_{\text{sources}}} R_{hkgj}R_{eldi}\left\langle \widehat{x}_{gj}(f)\widehat{x}_{di}^*(f) \right\rangle. \tag{21}$$

Now, by assuming that the actual brain sources are independent among them, we have that all terms $<\widehat{x}_{gj}(f)\widehat{x}_{di}^*(f)>$ with $j \neq i$ are equal to zero. In fact, these terms can be written as the product between $<\widehat{x}_{gj}(f)>$ and $\langle\widehat{x}_{di}^*(f)\rangle$, which are both equal to zero. Furthermore, by assuming that all the components of the same brain source are independent among them or that they have a pairwise phase difference equal to zero, it holds that $\langle\widehat{x}_{gi}(f)\widehat{x}_{di}^*(f)\rangle \in \mathbf{R}$. Thus, equation (21) becomes equal to

$$\sum_{h=1}^{3}\sum_{e=1}^{3} T_{hk}T_{gl} \sum_{g=1}^{3}\sum_{d=1}^{3}\sum_{i=1}^{N_{\text{sources}}} R_{hkgi}R_{eldi}\left\langle \widehat{x}_{gi}(f)\widehat{x}_{di}^*(f) \right\rangle, \tag{22}$$

which is a real number.

Appendix B. MPSI is invariant under invertible linear static transformations of the data

Let W_A and W_B be two linear and invertible spatial transformations of the data spaces A and B. We will in the following show that the MPSI_{AB} between the multivariate time series Z_A and Z_B coincides with the $\text{MPSI}_{\tilde{A}\tilde{B}}$ between $W_A Z_A$ and $W_B Z_B$. This statement follows from

$$
\begin{aligned}
\text{MPSI}_{\tilde{A}\tilde{B}} = 4 \cdot \sum_{f \in F} \text{tr}\Big(\big(W_A S_{AA}^R(f) W_A^t + W_A S_{AA}^R(f + \mathrm{d}f) W_A^t \big)^{-1} \\
\big(W_A S_{AB}^I(f + \mathrm{d}f) W_B^t \big) \big(W_B S_{BB}^R(f) W_B^t + W_B S_{BB}^R(f + \mathrm{d}f) W_B^t \big)^{-1} \\
\big(W_B S_{BA}^R(f) W_A^t \big) \Big) + 4 \cdot \sum_{f \in F} tr \big(W_A S_{AA}^R(f) W_A^t + W_A S_{AA}^R(f + \mathrm{d}f) W_A^t \big)^{-1} \\
\big(W_A S_{AB}^R(f + \mathrm{d}f) W_B^t \big) \big(W_B S_{BB}^R(f) W_B^t + W_B S_{BB}^R(f + \mathrm{d}f) W_B^t \big)^{-1} \\
\big(W_B S_{BA}^I(f) W_A^t \big) \Big) + 4 \cdot \sum_{f \in F} tr \Big(\big(S_{AA}^R(f) + S_{AA}^R(f + \mathrm{d}f) \big)^{-1} S_{AB}^I(f + \mathrm{d}f) \\
\big(S_{BB}^R(f) + S_{BB}^R(f + \mathrm{d}f) \big)^{-1} S_{BA}^R(f) + \big(S_{AA}^R(f) + S_{AA}^R(f + \mathrm{d}f) \big)^{-1} S_{AB}^R(f + \mathrm{d}f) \\
\big(S_{BB}^R(f) + S_{BB}^R(f + \mathrm{d}f) \big)^{-1} S_{BA}^I(f) \Big) = \text{MPSI}_{AB},
\end{aligned}
\tag{23}
$$

where we have used that

$$
\big(W_A S_{AA}^R(f) W_A^t + W_A S_{AA}^R(f + \mathrm{d}f) W_A^t \big)^{-1} = \big(W_A \big(S_{AA}^R(f) + S_{AA}^R(f + \mathrm{d}f) \big) W_A^t \big)^{-1} = \big(W_A^t \big)^{-1} \big(S_{AA}^R(f) + S_{AA}^R(f + \mathrm{d}f) \big)^{-1} W_A^{-1}
\tag{24}
$$

and the same for B.

References

Baccalá, L.A., Sameshima, K., 2001. Partial directed coherence: a new concept in neural structure determination. Biol. Cybern. 84, 463–474.

Basti, A., Pizzella, V., Nolte, G., Chella, F., Marzetti, L., 2017. Disclosing brain functional connectivity from electrophysiological signals with phase slope based metrics. J. serbian Soc. Comput. Mech. 11, 50–62.

Bastos, A.M., Vezoli, J., Fries, P., 2015. Communication through coherence with inter-areal delays. Curr. Opin. Neurobiol. 31, 173–180.

Blinowska, K.J., Kuś, R., Kamiński, M., 2004. Granger causality and information flow in multivariate processes. Phys. Rev. E 70, 050902.

Brookes, M.J., Woolrich, M., Luckhoo, H., Price, D., Hale, J.R., Stephenson, M.C., Barnes, G.R., Smith, S.M., Morris, P.G., 2011. Investigating the electrophysiological basis of resting state networks using magnetoencephalography. Proc. Natl. Acad. Sci. 108, 16783–16788.

Brookes, M.J., Woolrich, M.W., Barnes, G.R., 2012. Measuring functional connectivity in meg: a multivariate approach insensitive to linear source leakage. Neuroimage 63, 910–920.

Bullmore, E., Sporns, O., 2009. Complex brain networks: graph theoretical analysis of structural and functional systems. Nat. Rev. Neurosci. 10, 186–198.

Cavanna, A.E., Trimble, M.R., 2006. The precuneus: a review of its functional anatomy and behavioural correlates. Brain 129, 564–583.

Colclough, G., Brookes, M.J., Smith, S.M., Woolrich, M.W., 2015. A symmetric multivariate leakage correction for meg connectomes. NeuroImage 117, 439–448.

Colclough, G., Woolrich, M., Tewarie, P., Brookes, M., Quinn, A., Smith, S., 2016. How reliable are meg resting-state connectivity metrics? NeuroImage 138, 284–293.

Corbetta, M., Shulman, G.L., 2002. Control of goal-directed and stimulus-driven attention in the brain. Nat. Rev. Neurosci. 3, 201–215.

Deco, G., Corbetta, M., 2011. The dynamical balance of the brain at rest. Neurosci 17, 107–123.

Deco, G., Tononi, G., Boly, M., Kringelbach, M.L., 2015. Rethinking segregation and integration: contributions of whole-brain modelling. Nat. Rev. Neurosci. 16, 430–439.

Dosenbach, N.U., Fair, D.A., Cohen, A.L., Schlaggar, B.L., Petersen, S.E., 2008. A dual-networks architecture of top-down control. Trends cognitive Sci. 12, 99–105.

Engel, A.K., Gerloff, C., Hilgetag, C.C., Nolte, G., 2013. Intrinsic coupling modes: multiscale interactions in ongoing brain activity. Neuron 80, 867–886.

Ewald, A., Marzetti, L., Zappasodi, F., Meinecke, F.C., Nolte, G., 2012. Estimating true brain connectivity from eeg/meg data invariant to linear and static transformations in sensor space. Neuroimage 60, 476–488.

Fox, M.D., Snyder, A.Z., Vincent, J.L., Corbetta, M., Van Essen, D.C., Raichle, M.E., 2005. The human brain is intrinsically organized into dynamic, anticorrelated functional networks. Proc. Natl. Acad. Sci. U. S. A. 102, 9673–9678.

Fries, P., 2015. Rhythms for cognition: communication through coherence. Neuron 88, 220–235.

Geweke, J., 1982. Measurement of linear dependence and feedback between multiple time series. J. Am. Stat. Assoc. 77, 304–313.

Granger, C.W., 1969. Investigating causal relations by econometric models and cross-spectral methods. Econ. J. Econ. Soc. 424–438.

Hacker, C.D., Laumann, T.O., Szrama, N.P., Baldassarre, A., Snyder, A.Z., Leuthardt, E.C., Corbetta, M., 2013. Resting state network estimation in individual subjects. Neuroimage 82, 616–633.

Heekeren, H.R., Marrett, S., Ruff, D.A., Bandettini, P., Ungerleider, L.G., 2006. Involvement of human left dorsolateral prefrontal cortex in perceptual decision making is independent of response modality. Proc. Natl. Acad. Sci. 103, 10023–10028.

Hillebrand, A., Tewarie, P., van Dellen, E., Yu, M., Carbo, E.W., Douw, L., Gouw, A.A., van Straaten, E.C., Stam, C.J., 2016. Direction of information flow in large-scale resting-state networks is frequency-dependent. Proc. Natl. Acad. Sci. 113, 3867–3872.

Hipp, J.F., Hawellek, D.J., Corbetta, M., Siegel, M., Engel, A.K., 2012. Large-scale cortical correlation structure of spontaneous oscillatory activity. Nat. Neurosci. 15, 884–890.

Hotelling, H., 1936. Relations between two sets of variates. Biometrika 28, 321–377.

Larson-Prior, L.J., Oostenveld, R., Della Penna, S., Michalareas, G., Prior, F., Babajani-Feremi, A., Schoffelen, J.-M., Marzetti, L., de Pasquale, F., Di Pompeo, F., et al., 2013. Adding dynamics to the human connectome project with meg. Neuroimage 80, 190–201.

Mantini, D., Penna, S.D., Marzetti, L., de Pasquale, F., Pizzella, V., Corbetta, M., Romani, G.L., 2011. A signal-processing pipeline for magnetoencephalography resting-state networks. Brain connect. 1, 49–59.

Marinazzo, D., Pellicoro, M., Stramaglia, S., 2008. Kernel method for nonlinear granger causality. Phys. Rev. Lett. 100, 144103.

Marzetti, L., Del Gratta, C., Nolte, G., 2008. Understanding brain connectivity from eeg data by identifying systems composed of interacting sources. Neuroimage 42, 87–98.

Marzetti, L., Della Penna, S., Snyder, A.Z., Pizzella, V., Nolte, G., de Pasquale, F., Romani, G.L., Corbetta, M., 2013. Frequency specific interactions of meg resting state activity within and across brain networks as revealed by the multivariate interaction measure. Neuroimage 79, 172–183.

Marzetti, L., Di Lanzo, C., Zappasodi, F., Chella, F., Raffone, A., Pizzella, V., 2014. Magnetoencephalographic alpha band connectivity reveals differential default mode network interactions during focused attention and open monitoring meditation. Front. Hum. Neurosci. 8, 832.

Nolte, G., 2003. The magnetic lead field theorem in the quasi-static approximation and its use for magnetoencephalography forward calculation in realistic volume conductors. Phys. Med. Biol. 48, 3637.

Nolte, G., Bai, O., Wheaton, L., Mari, Z., Vorbach, S., Hallett, M., 2004. Identifying true brain interaction from eeg data using the imaginary part of coherency. Clin. Neurophysiol. 115, 2292–2307.

Nolte, G., Marzetti, L., Sosa, P.V., 2009. Minimum overlap component analysis (moca) of eeg/meg data for more than two sources. J. Neurosci. methods 183, 72–76.

Nolte, G., Ziehe, A., Krämer, N., Popescu, F., Müller, K.-R., 2010. Comparison of granger causality and phase slope index. In: NIPS Causality: Objectives and Assessment, pp. 267–276.

Nolte, G., Ziehe, A., Nikulin, V.V., Schlögl, A., Krämer, N., Brismar, T., Müller, K.-R., 2008. Robustly estimating the flow direction of information in complex physical systems. Phys. Rev. Lett. 100, 234101.

ONeill, G.C., Barratt, E.L., Hunt, B.A., Tewarie, P.K., Brookes, M.J., 2015. Measuring electrophysiological connectivity by power envelope correlation: a technical review on meg methods. Phys. Med. Biol. 60, R271.

Oostenveld, R., Fries, P., Maris, E., Schoffelen, J.-M., 2011. Fieldtrip: open source software for advanced analysis of meg, eeg, and invasive electrophysiological data. Comput. Intell. Neurosci. 2011, 1.

Palva, S., Palva, J.M., 2012. Discovering oscillatory interaction networks with m/eeg: challenges and breakthroughs. Trends cognitive Sci. 16, 219–230.

Pascual-Marqui, R.D., Lehmann, D., Koukkou, M., Kochi, K., Anderer, P., Saletu, B., Tanaka, H., Hirata, K., John, E.R., Prichep, L., et al., 2011. Assessing interactions in

the brain with exact low-resolution electromagnetic tomography. Philosophical Transactions of the Royal Society of London A: Mathematical Phys. Eng. Sci. 369, 3768–3784.

de Pasquale, F., Della Penna, S., Snyder, A.Z., Lewis, C., Mantini, D., Marzetti, L., Belardinelli, P., Ciancetta, L., Pizzella, V., Romani, G.L., et al., 2010. Temporal dynamics of spontaneous meg activity in brain networks. Proc. Natl. Acad. Sci. 107, 6040–6045.

de Pasquale, F., Della Penna, S., Snyder, A.Z., Marzetti, L., Pizzella, V., Romani, G.L., Corbetta, M., 2012. A cortical core for dynamic integration of functional networks in the resting human brain. Neuron 74, 753–764.

de Pasquale, F., Marzetti, L., 2014. Temporal and spectral signatures of the default mode network. In: Magnetoencephalography. Springer, pp. 451–476.

Riesenhuber, M., Poggio, T., 1999. Hierarchical models of object recognition in cortex. Nat. Neurosci. 2, 1019–1025.

Rubinov, M., Sporns, O., 2010. Complex network measures of brain connectivity: uses and interpretations. Neuroimage 52, 1059–1069.

Slepian, D., 1978. Prolate spheroidal wave functions, fourier analysis, and uncertaintyv: the discrete case. Bell Labs Tech. J. 57, 1371–1430.

Smith, S.M., Fox, P.T., Miller, K.L., Glahn, D.C., Fox, P.M., Mackay, C.E., Filippini, N., Watkins, K.E., Toro, R., Laird, A.R., et al., 2009. Correspondence of the brain's

functional architecture during activation and rest. Proc. Natl. Acad. Sci. 106, 13040–13045.

Soto, J.L., Lachaux, J.-P., Baillet, S., Jerbi, K., 2016. A multivariate method for estimating cross-frequency neuronal interactions and correcting linear mixing in meg data, using canonical correlations. J. Neurosci. methods 271, 169–181.

Sporns, O., 2013. Network attributes for segregation and integration in the human brain. Curr. Opin. Neurobiol. 23, 162–171.

Tong, F., 2004. Representations of visual imagery in human primary visual cortex. J. Vis. 4, 46.

Tzourio-Mazoyer, N., Landeau, B., Papathanassiou, D., Crivello, F., Etard, O., Delcroix, N., Mazoyer, B., Joliot, M., 2002. Automated anatomical labeling of activations in spm using a macroscopic anatomical parcellation of the mni mri single-subject brain. Neuroimage 15, 273–289.

Varela, F., Lachaux, J.-P., Rodriguez, E., Martinerie, J., 2001. The brainweb: phase synchronization and large-scale integration. Nat. Rev. Neurosci. 2, 229–239.

Vinck, M., Oostenveld, R., Van Wingerden, M., Battaglia, F., Pennartz, C.M., 2011. An improved index of phase-synchronization for electrophysiological data in the presence of volume-conduction, noise and sample-size bias. Neuroimage 55, 1548–1565.

Vossel, S., Geng, J.J., Fink, G.R., 2014. Dorsal and ventral attention systems distinct neural circuits but collaborative roles. Neurosci 20, 150–159.